Nanocrystalline Tin dioxide thin films as oxidising gas sensors

Juan A. de Agapito, José P. Santos, Miguel A. Martín and Hernán Vásquez*

Departamento de Electrónica, Facultad de Ciencias Físicas, Universidad Complutense de Madrid, Ciudad Universitaria, 28040 Madrid, Spain
Phone +34 1 3944441 e-mail: agapito@fis.ucm.es
**Facultad de Ciencias Físicas, Universidad Nacional de Ingeniería, Lima, Perú*

Abstract

Nanocrystalline tin dioxide has been employed to develop two types of sensor devices. Two electrical properties, resistivity and work function, increase with oxidising gas adsorption. The first leads to the classical thin film resistive sensor. The other property is used to design a switching diode. Both devices show a high sensitivity and linearity under proper design and operating parameters. Typical figures are 100 % resistance change and 50 mV voltage shift for 50 ppb of NO_2 in air. A theoretical model is proposed to explain the results.

I. Introduction

The monitoring of oxidising gases (as NO_2) is of great importance for urban air quality. Tin dioxide sensors are good candidates for this task. Their operation principle lies in capture of conduction electrons by the adsorbed gas molecules [1].

The existence of charge trapping in the surface states due to adsorption has two consequences on the electrical properties of the material: variation of the conductivity and the work function [2]. These changes can be used to design two types of sensors: resistive sensors and structured sensors.

II. Model

First of all we have to modelise the semiconductor. The necessary assumptions to calculate the variations of electrical properties with gas concentration are:

1. The semiconductor thin film is composed by identical crystallites of radius R.
2. The hole concentration can be neglected because SnO_2 is a wide band gap n-type semiconductor [3].

3. Conduction band electrons are captured only by the surface sates created by chemisorption.
4. Oxygen vacancies act as double donors with energies E_{D1} = 30 and E_{D2} = 150 meV below the conduction band edge [4].
5. The crystallite surface is homogeneous and the gas has access to all of it.
6. There is no interaction between adsorbed molecules.

The problem is not too difficult when the grain size is large enough so that the space charge region does not extend to the whole grain. In this case the surface properties are not affected by bulk properties.

The second condition means that adsorption properties of the surface are independent of the Fermi level.

A Langmuir adsorption isotherm is commonly used [5]. In the case that the Fermi level position affects the properties of the surface Volkenstein isotherm has to be used [6]:

$$\theta = \frac{\beta P}{1+\beta P} \tag{1}$$

Where θ is the surface coverage of gas species, P is the partial pressure of the gas and β is the coefficient of the Volkenstein isotherm given by

$$\beta = b\left\{ f^0 \left[1+\frac{\nu^-}{\nu^0}\exp\left(\frac{E_t^f - E_c}{kT} \right) \right] \right\} \tag{2}$$

Where b is the Langmuir isotherm coefficient, ν^- and ν^0 are phononic frequencies, E_t^f is the effective surface level created by the adsorbed molecule, k is the Bolztmann constant, T is the absolute temperature and f^0 is the occupation probability of the weak chemisorbed state

$$f^0 = \frac{1}{1+\exp\left(\frac{E_F - E_t^f}{kT} \right)} \tag{3}$$

The total charge density at the surface is given by

$$N^- = N_{ad}\theta(1-f^0) \tag{4}$$

Where N_{ad} is the adsorption sites density.

For several species competing for the adsorption sites one has to developed a multispecies adsorption model [7] for several oxidising species competing for the same number of chemisorption centres. The charge density at the surface is in this case

$$N^- = \sum_i N_{ad}\theta_i\left(1 - f_i^0\right) \tag{5}$$

For each specie i

$$\theta_i = \frac{\beta_i P_i}{1 + \sum_{j=1}^{k} \beta_j P_j} \tag{6}$$

Now we have the surface charge density as a function of the partial pressure gas and we can solve Poisson equation in order to calculate potential distribution and carrier concentration in the crystallite. For spherical co-ordinates and considering only r dependence

$$\frac{d^2\xi(r)}{dr^2} + \frac{2}{r}\frac{d\xi(r)}{dr} = -\frac{q^2}{\varepsilon kT}\left[n(r) - N_D^+(r)\right] \tag{7}$$

Where

$$\xi(r) = \frac{\left[E_c(r) - E_F\right]}{kT} \tag{8}$$

$Ec(r)$ is the position of the conduction band, E_F is the Fermi level, q is the electronic charge, ε is the dielectric constant of the material, $n(r)$ the point carrier density and N_D^+ the ionised donor density given by

$$n(r) = \frac{2N_c}{\sqrt{\pi}} F_{1/2}(-\xi) \tag{9}$$

$$N_D^+ \cong N_D\left[\frac{1}{1 + 2\exp\left[-\left(\varepsilon_{D1} - \xi(r)\right)\right]} + \frac{1}{1 + 2\exp\left[-\left(\varepsilon_{D2} - \xi(r)\right)\right]}\right] \tag{10}$$

Where N_c is the effective density of states at the conduction bandedge, $F_{1/2}$ is the Fermi-Dirac integral, N_D is the vacancy density (assumed uniformly distributed) and ε_{Di} are the reduced donor levels [$\varepsilon_{Di} = (E_C - E_{Di})/kT$].

If the crystallite is small we can not use the initial condition $\xi = 0$ for $r = 0$ because the depletion zone is extended over the whole grain and thus the conduction band is shifted away the Fermi level. However, for symmetry considerations, the electric field in the centre of the grain is zero:

$$\left.\frac{d\xi}{dr}\right|_{r=0} = 0 \tag{11}$$

The boundary conditions are Gauss's Law and charge neutrality that can be grouped together in

$$\left.\frac{d\xi}{dr}\right|_{r=R} = \frac{q^2}{2\varepsilon kT}\sum N_i^-(P,\xi(r)) \tag{12}$$

The boundary condition for this equation depends on the solution of eq. (7) hence Poisson equation has to be solved self-consistently.

For this model we have used three variables (R, N_{ad} and E_t) and the following fixed parameters

Table 1

Parameter	Value
ε_r	13.5
E_{D1}-E_C	30 meV
E_{D2}-E_C	150 meV
N_D	10^{19} cm^{-3}
ν^0,ν^-	10^{13} s^{-1}
β_{O2}	1.36 x 10^{-3} Pa^{-1}
β_{NO_2}	2.85 Pa^{-1}
E_{O_2}-E_C	0.6 eV

The Poisson equation has been solved with a program that uses fourth order Runge-Kutta algorithm with an iterative shooting method (See annex for mathematical details). In fig. 1 the reduced potential is shown in pure air and in air with four different NO_2 concentrations for two grains 65 Å diameter at 180 °C (only the two halves are shown). The NO_2 energy level used for the calculation is 1.06 eV below the conduction band edge and the density of adsorption sites is 2.17 x 10^{12} cm^{-3}. These are within the same order of magnitude of the density of oxygen vacancies at the surface (assuming a uniform distribution). We have to note that the intracrystallite potential barrier is as low as 55 mV and that the whole conduction band has shifted upwards with respect to its position in vacuum (4 meV at 180 °C). For example, for 200 ppb of NO_2, the model predicts a shift of 140 meV with respect to pure air.

III. Resistive sensors

For the resistive sensors one has to find a relationship between conductivity changes and partial pressures (or concentrations) of the gas. The classical expression for the conductivity is

$$\sigma = qn\mu \tag{13}$$

If we can neglect the contribution of the mobility changes, and there are experimental evidences of a small contribution [8], the sensitivity to an oxidising gas is given by

$$S \equiv \frac{n_0}{n_{eff}} \tag{14}$$

where n_0 is the effective carrier concentration in the absence of the test gas and n_{eff} is the effective carrier concentration in the presence of the gas. The effective carrier concentration is obtained integrating the point carrier concentration in the whole grain and dividing for its size

$$n_{eff} = \frac{1}{V}\int_v n(r)dr \tag{15}$$

IV. Structured sensors

A switching tunnel device has been designed based on a MIS switching diode [9]. A metal, a thin insulator layer 100 Å, an epitaxial n semiconductor region and a p^+ semiconductor region compose the diode. The I-V characteristic of this diode presents three regions: high impedance, negative resistance and low impedance zones (fig.2).

Forward polarisation induces electron-hole pairs to be generated in the epitaxial n-layer. The electrons are swept to the p-n junction and the holes begin to accumulate at the oxide - epitaxial layer interface. The current in zone A-B of fig. 2 is mainly due to recombination processes. The corresponding band diagram is sketched in fig. 3. The width of the depletion zone is given by:

$$X_d = \left(2\varepsilon_s\phi_s / qN_D\right)^{1/2} \tag{16}$$

ε_s, ϕ_s and N_d being the dielectric constant, surface potential and donor density, respectively. The tunnelling probability is strongly dependent on the insulator thickness [10]. The total potential across the device may be written as:

$$V = V_{ox} + \phi_s + V_j \tag{17}$$

where V_{ox} is the voltage across the oxide and V_j the voltage drop across the junction. It can be shown that under the condition used here (d_{ox} ~ 50 Å, N_D ~ 2 x 10^{14} cm^{-3}) V_{ox} represents only a few percent of ϕ_s. On the other hand V_j is small due to the low current involved. Therefore it is possible to write:

$$V \cong \phi_s \tag{18}$$

As voltage increases further, X_d extend to the junction [15]:

$$X_d = W_n - W_j \tag{19}$$

where W_n and W_j are the widths of the epitaxial layer and of the depleted zone of the junction, respectively. At this point the "punchthrough" conditions are stablished. The switching voltage (point B) correspond to the value:

$$V = V_{BF} \approx \phi_{PT} = \frac{qN_D(W_n - W_j)^2}{2\varepsilon_s} \tag{20}$$

For a more rigorous treatment one has to consider the differences in work functions between the metal and the semiconductor and modify the switching voltage accordingly:

$$V_{BF} = \phi_{PT} + \phi_{ms} \tag{21}$$

Punchtrough results in the lowering of the junction barrier driving an injection of holes towards the epitaxial layer. The electric field across the insulator is so low that the large injected hole current cannot tunnel through and a significant accumulation of holes take place. Such accumulation results in two interacting phenomena:

(i) the *n*-layer moves towards inversion and therefore ϕs and the voltage across the device decrease,

(ii) the electric field in the insulator increases allowing significantly higher electron tunnelling to occur.

The overall result is the region of negative resistance (B-C).

Substituting the metal with tin dioxide one can take advantage of the change of work function with the adsorption of the oxidising species. The presence of NO_2 should be detectable as a shift in V_{BF}. Thus we can obtain a switch controlled by the partial pressure of the gas [11].

IV. Results

Resistive sensors

We have calculated the calibration curves (conductivity changes vs. partial pressure) of oxygen in nitrogen and nitrogen dioxide in air for a series of thin film nanocrystalline SnO_2 sensors. Sensors were prepared by reactive sputtering at different temperatures and oxygen partial pressure [12]. Film thickness between 2990 and 5000 Å were obtained. After deposition, the samples underwent a thermal treatment for a period of 12h at 375 °C to stabilise the defects concentration and distribution. GAXRD analysis showed that the films were nanocrystallines with crystallite sizes between 2 and 15 nm. Auger depth profile analysis (AES) confirmed the thickness uniformity and the presence of impurities (mainly carbon) at the surface.

Electrical response of the sensors were measured in apparatus described elsewhere [13]. The operating temperatures varied between 100 and 350 °C, however below 150 °C the response was very slow. The concentration range was 0.5 -10 % in volume of oxygen in nitrogen and 50-800 ppb of NO_2 in air.

In the oxygen partial pressure range studied the sensitivity followed a power law trend. Theoretical calculations are in excellent agreement with the results. The only parameters allowed to change at each temperature are the number of chemisorption sites and surface energy level created by the adsorption of oxygen [14].

For NO_2 in air the calibration curves followed two trends: power law behaviour and parabolic or saturation behaviour (fig.4). Theory is in excellent agreement with experiments, if the number of adsorption sites and the energy level created by NO_2 adsorption are allowed to change with temperature. The density of chemisorption sites is found to be, in all cases, of the same order of magnitude of the oxygen vacancies at the surface, so we can conclude that these are the chemisorption centres.

Structured sensors

The devices have been prepared with p^+ silicon wafer with *n*-epitaxial layer as a starting material. Typically such junctions are covered with a 20-40 Å thick native oxide. SnO_2 thin nanocrystalline layers (200 to 1700 Å) are deposited on top of this substrate. The average grain size measured by GAXRD was found to be 70 ± 20 Å.

Depending on the native oxide thickness we have found three types of behaviours [11]: MOS diode for thick oxides, switch tunnel diode for intermediate thickness and normal

diode for thin oxides. Some sensors exhibit a linear response (switching voltage vs. concentration) in a wide concentration range (fig. 5) and others showed a saturation of the switching voltage for high concentrations. Some problems of reversibility arose because of the low operating temperatures. Calculations for the sensor of fig. 5 gave a 140 meV work function shift for 200 ppb of NO_2 with the parameters of table I. The measured switching voltage increment for this concentration is ~ 160 mV .

V. Conclusions

Nanocrystalline thin tin dioxide films are extremely sensitive to very low oxidising gas concentrations. The generalised Volkenstein isotherm based model can account for the experimental data observed. The most important parameter for these nanocrystalline sensors is the number of chemisorption sites at the surface. This parameter is very dependent of the sensor preparation so extreme care must be taken in order to obtain reproducible responses. The switching device is very promising as an alternative to the conventional resistive sensors.

Annex

From the original second order differential equation two first order differential equation are obtained:

$$\frac{dy_1(r)}{dr} = \frac{d\xi(r)}{dr} = \frac{y_2(r)}{r}$$

$$\frac{dy_2(r)}{dr} = -\left\{\frac{y_2(r)}{r} + \frac{q^2 r}{\varepsilon kT}\frac{2N_c F_{1/2}(y_1)}{\sqrt{\pi}} - N_D\left[\frac{1}{1+2\exp(-(\varepsilon_{D1}+y_1))} + \frac{1}{1+2\exp(-(\varepsilon_{D2}+y_1))}\right]\right\} \quad \text{(A 1)}$$

To each equation the fourth order Runge-Kutta formula [15] is applied:

$$y_{n+1} = y_n + \frac{k_1}{6} + \frac{k_2}{3} + \frac{k_3}{3} + \frac{k_4}{6} \quad \text{(A 2)}$$

with

$$k_1 = hf'(x_n, y_n)$$

$$k_2 = hf'\left(x_n + \frac{h}{2}, y_n + \frac{k_1}{2}\right) \quad \text{(A 3)}$$

$$k_3 = hf'\left(x_n + \frac{h}{2}, y_n + \frac{k_2}{2}\right)$$

$$k_4 = hf'(x_n + h, y_n + k_3)$$

where h is the step size and f' is the right hand of equation (A 1).

We only know the initial condition for one of the variables (y_2) so we have to use a "shooting method" where the integration proceeds from *0* to *R* and try to match boundary conditions at the end of the integration.

$$y_2(R) = \frac{Rq^2}{2\varepsilon kT} \sum N_i^-(P, y_1(R)) \qquad \text{(A 4)}$$

The shooting method implements multidimensional Newton-Raphson [16] to find the zeros of the functions obtained integrating the differential equations.

We generate an initial value *V* and obtain through integration $y_2(R)$.

At this point we define a discrepancy factor

$$F = y_2(R) - \frac{Rq^2}{2\varepsilon kT} \sum N_i^-(P, y_1(R)) \qquad \text{(A 5)}$$

So we have to find a value V that zeros F. We do this by computing the solution of the equation

$$\alpha \cdot \delta V = -F \qquad \text{(A 6)}$$

and then adding the correction back

$$V^{new} = V^{old} + \delta V \qquad \text{(A 7)}$$

where

$$\alpha = \frac{dF}{dV} \approx \frac{F(V + \Delta V) - F(V)}{\Delta V} \qquad \text{(A 8)}$$

Once solved the equation and obtained the potential we can calculate the effective carrier density through (15) and the theoretical sensitivities S^t. If we know the experimental sensitivities we can define an error function

$$RMFS = \sqrt{\frac{1}{N} \sum_i \left(100 \times \frac{S_i^t - S_i^{ex}}{S_i^{ex}} \right)^2} \qquad \text{(A 9)}$$

where N is the number of concentration points at each temperature and S_i^{ex} are the measure sensitivities.

The problem now is to minimise a function of two variables E_{NO_2} and N_{ad}. We use the Downhill Simplex method to do this [17]. A simplex is the geometrical figure consisting, in N dimensions, of N+1 points and their interconnecting lines, faces, etc. In two dimensions is a triangle.

The method must be started with 3 points defining an initial simplex. If $\boldsymbol{P_0}$ is one of the starting points the other points are

$$\vec{P}_i = \vec{P}_0 + \lambda \vec{e}_i \qquad \text{(A 10)}$$

where e_i's are unit vectors and λ is a constant defining the problem characteristic length scale.

The downhill simplex method now takes a series of steps, most steps just moving the point of the simplex where the function is larger (high point) through the opposite face of the simplex to a lower point. This is called a reflection and is constructed to preserve the simplex volume (area in two dimensions). Other possible steps are: reflection and expansion away from the high point, contraction along one dimension from the high point and contractions along all dimensions to the low point. An appropriate sequence of these steps will always converge to a minimum of the function.

References

1. S. C. Chang, Oxygen chemisorption on tin oxide: correlation between electrical conductivity and EPR measurements. *J. Vac. Sci. Technol., 17* (1980) 366-369.
2. H. Geistlinger, Electron theory of thin film gas sensors. *Sensors and Actuators B, 17* (1993) 47-60.
3. J. Melsheimer and D. Ziegler, Ban gap energy and Urbah tail studies of amorphous partially crystalline and polycrystalline tin oxide. *Thin Solid Films, 129* (1985) 35.
4. S. Samson and C.G. Fondstad, Defect structure and electronic donor levels in stannic oxide crystals. *J. Appl. Phys., 44* (1973) 4618.
5. P. K. Clifford, . *Proc. 1st Int. Conf. Chemical Sensors, Fukuoka, Japan,* (1983).
6. Th. Volkenstein, *The electron theory of catalysis on semiconductors*, Pergamon Press, Oxford, (1963).
7. J. A. Agapito and J. P. Santos, The interaction of low NO_2 concentrations in air with degenerate nanocrystalline tin dioxide thin films. *Sensors and Actuators B, 31* (1996) 93-98.
8. F. J. Gutiérrez, L. Arés, J.I.Robla, J.M. Getino, M. C. Horrillo, I. Sayago and J.A. Agapito, Hall coefficient measurements for SnO_2 doped sensors, as a function of temperature and atmosphere. *Sensors and Actuators B, 15-16* (1993) 98-104.
9. J. G. Simmons and A. El-Badry, Theory of switching phenomena in metal/semi-insulator/n-p^+ Silicon devices. *Solid State Electron., 20* (1977) 955.
10. S. M. Sze, *Physics of semiconductor devices*, Wiley, New York, (1991).

11. G. B. Barbi, J. Santos Blanco, M. Baroffio, J. Agapito and F. J. Gutiérrez, An SnO_2 based switching tunnel device for the detection of NO_2 in air at the sub-ppm level. *Sensors and Actuators B, 18-19* (1994) 93-98.
12. M.C. Horrillo, P.Serrini, J. Santos and L. Manes, Influence of the deposition conditions of SnO_2 thin films by reactive sputtering on the sensitivity to urban pollutants. *Sensors and Actuators B, 45* (1997) 193-198.
13. G. B. Barbi, J. Santos Blanco, Structure of tin oxide layers and operating temperature as factors determining the sensitivities performances to NO_x. *Sensors and Actuators B, 15-16* (1993) 372-378.
14. J. Santos, P. Serrini, B. O'Beirn and L. Manes, A thin film SnO_2 gas sensor selective to ultra-low NO_2 concentrations in air. *Sensors and Actuators B, 43* (1997) 154-160.
15. J. R. Rice, *Numerical Methods, Software and Analysis*, Mc Graw Hill, New York, (1983).
16. F.S. Actorn, *Numerical Methods that works*, Harper and Row, New York, (1970).
17. J.A. Nelder and R. Mead, *Computer Journal, 7* (1965) 308.

Figure captions

Fig. 1 Intracrystallite potential for several NO_2 concentrations.

Fig. 2 Current- Voltage characteristics of a MIS switch diode. A-B high impedance region, B-C negative resistance region, C-D low impedance region.

Fig. 3 Energy band diagram of a forward-polarised MIS switch diode before punch-through.

Fig. 4 Experimental and theoretical sensitivities to low NO_2 concentrations.

Fig. 5 Switching voltage vs. NO_2 concentration for a tunnel diode sensor.

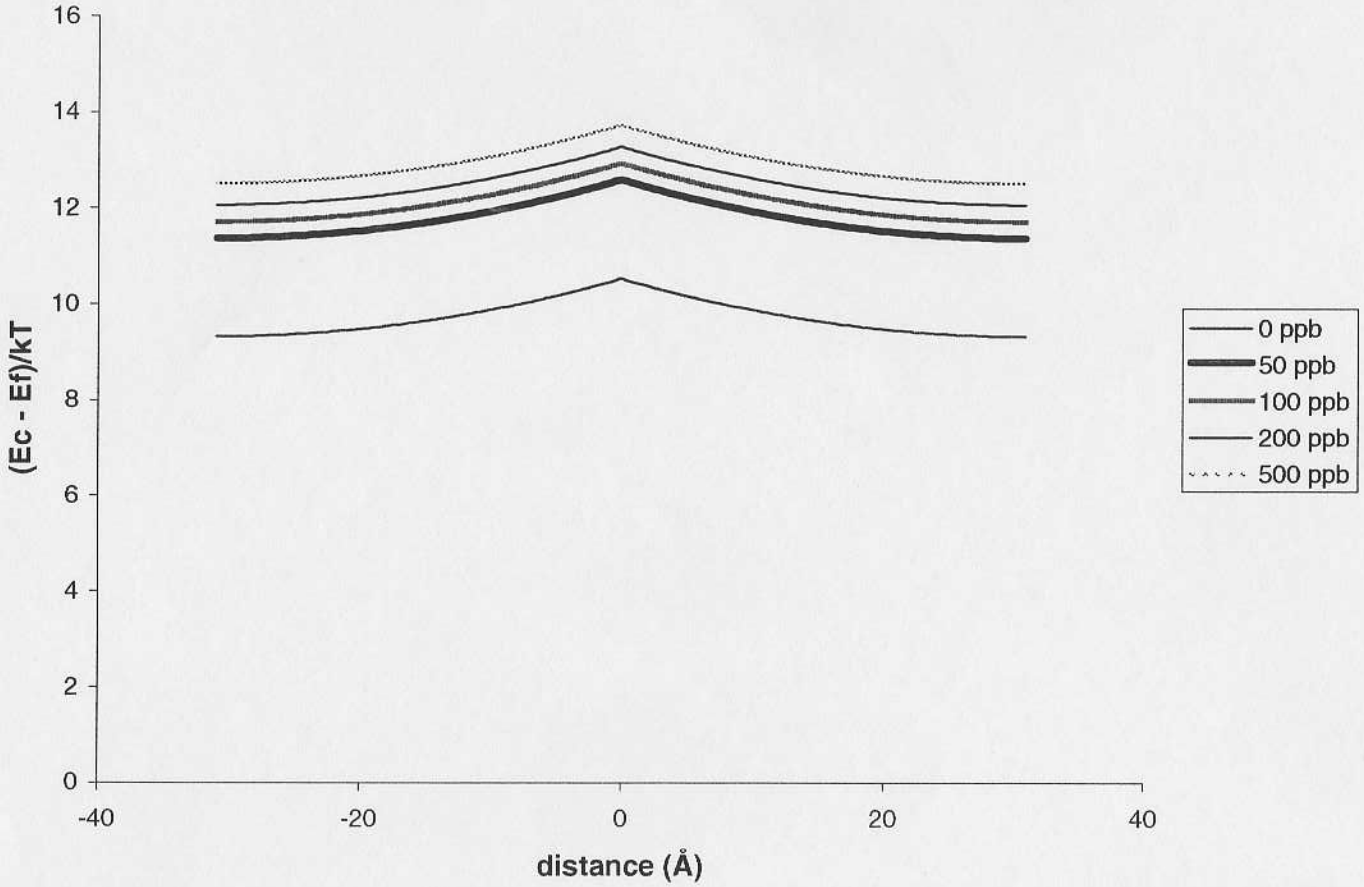
16
14
12
10
8
6
4
2
0
(Ec - Ef)/kT
-40
-20
0
20
40
distance (Å)
0 ppb
50 ppb
100 ppb
200 ppb
500 ppb

Figure 1

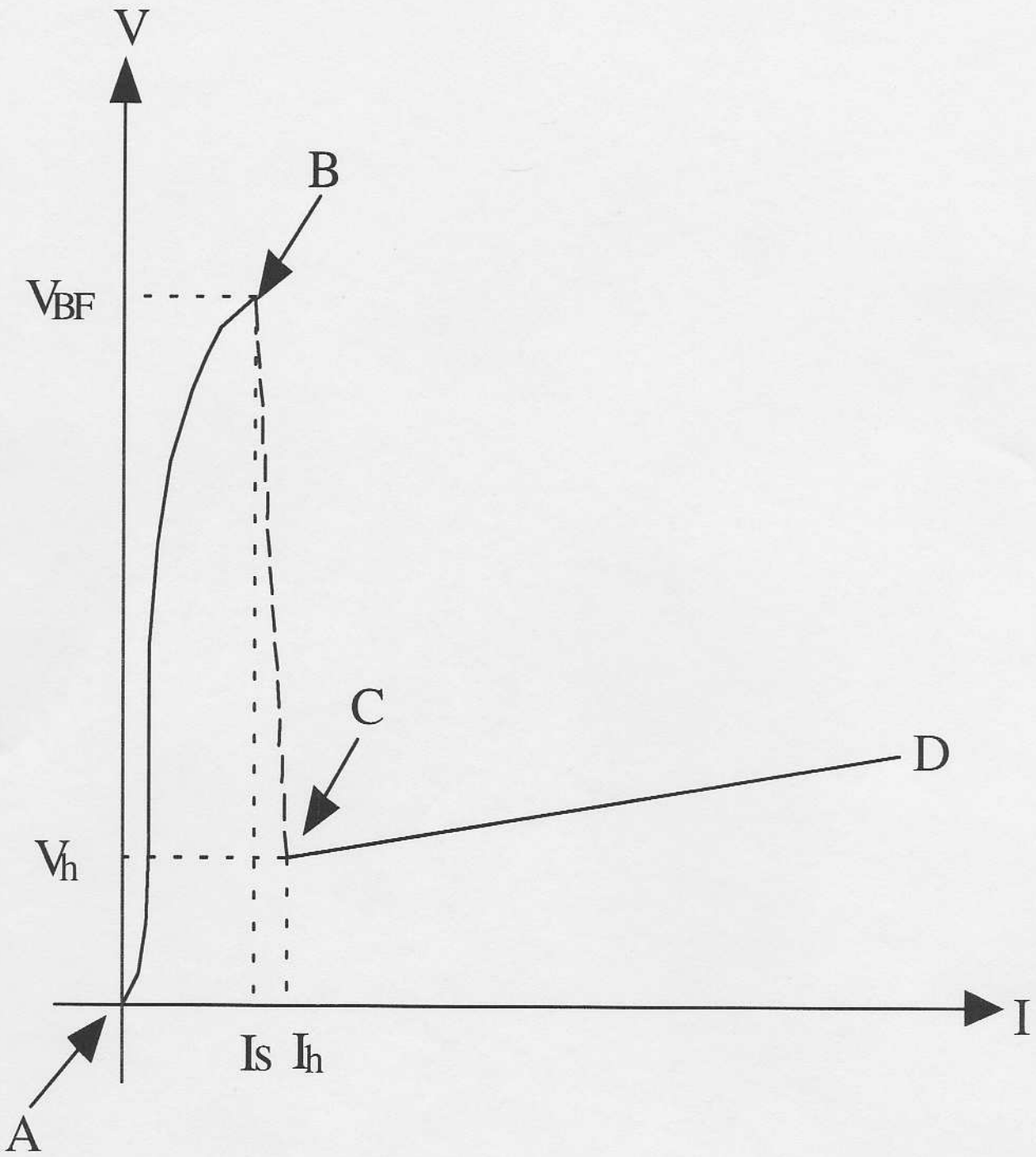

Figure 2

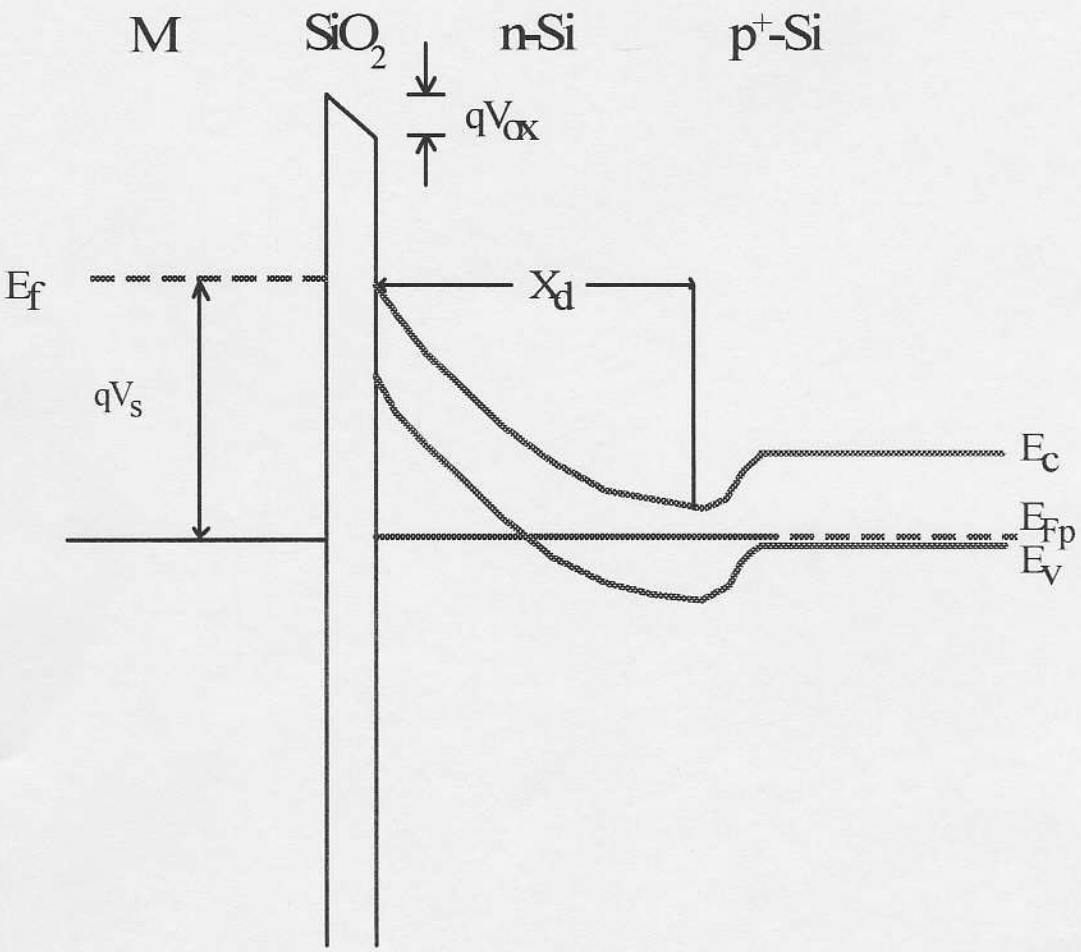

Figure 3

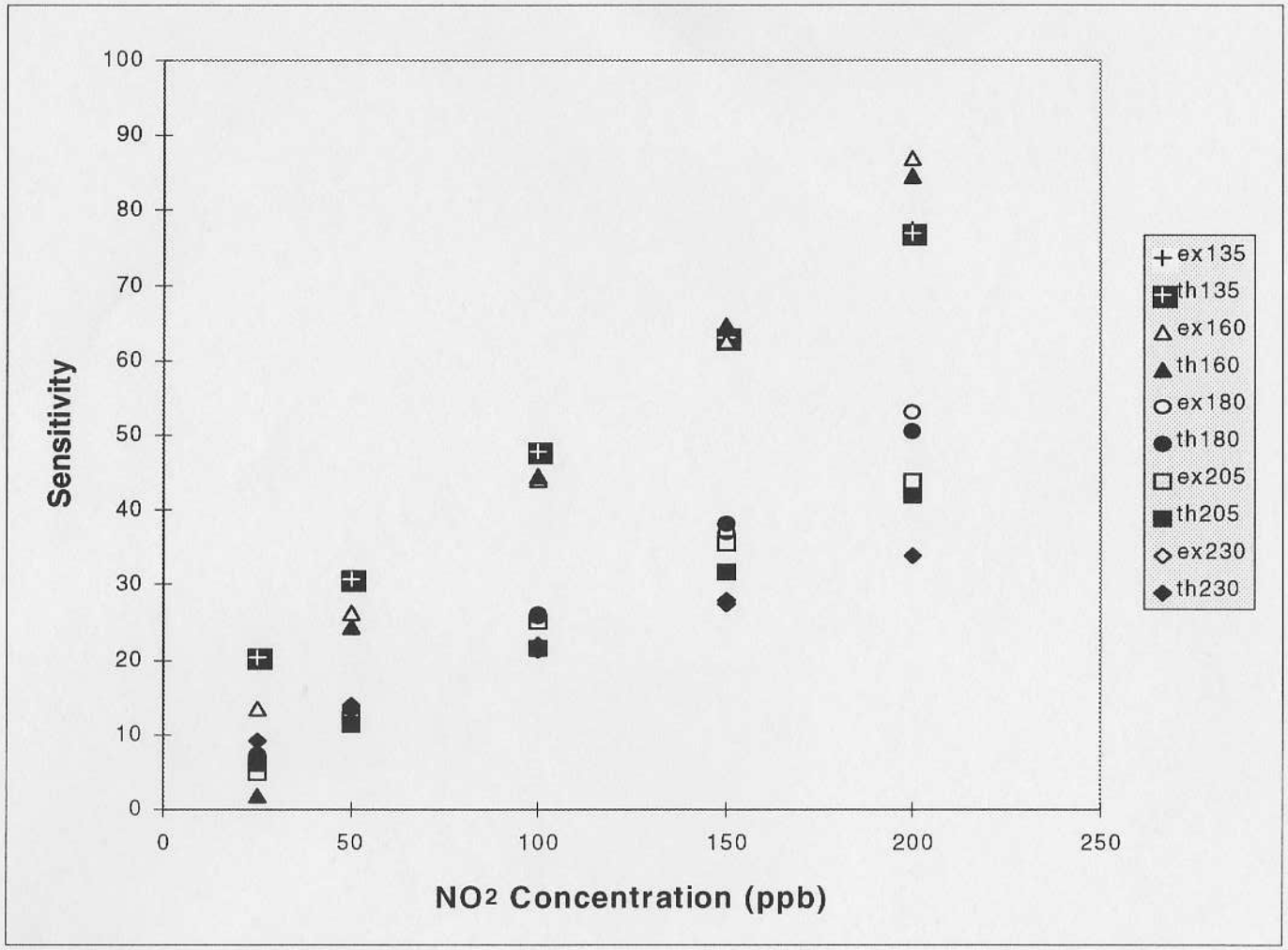
Sensitivity
100
90
80
70
60
50
40
30
20
10
0
0
50
100
150
200
250
NO2 Concentration (ppb)
ex135
th135
ex160
th160
ex180
th180
ex205
th205
ex230
th230

Figure 4

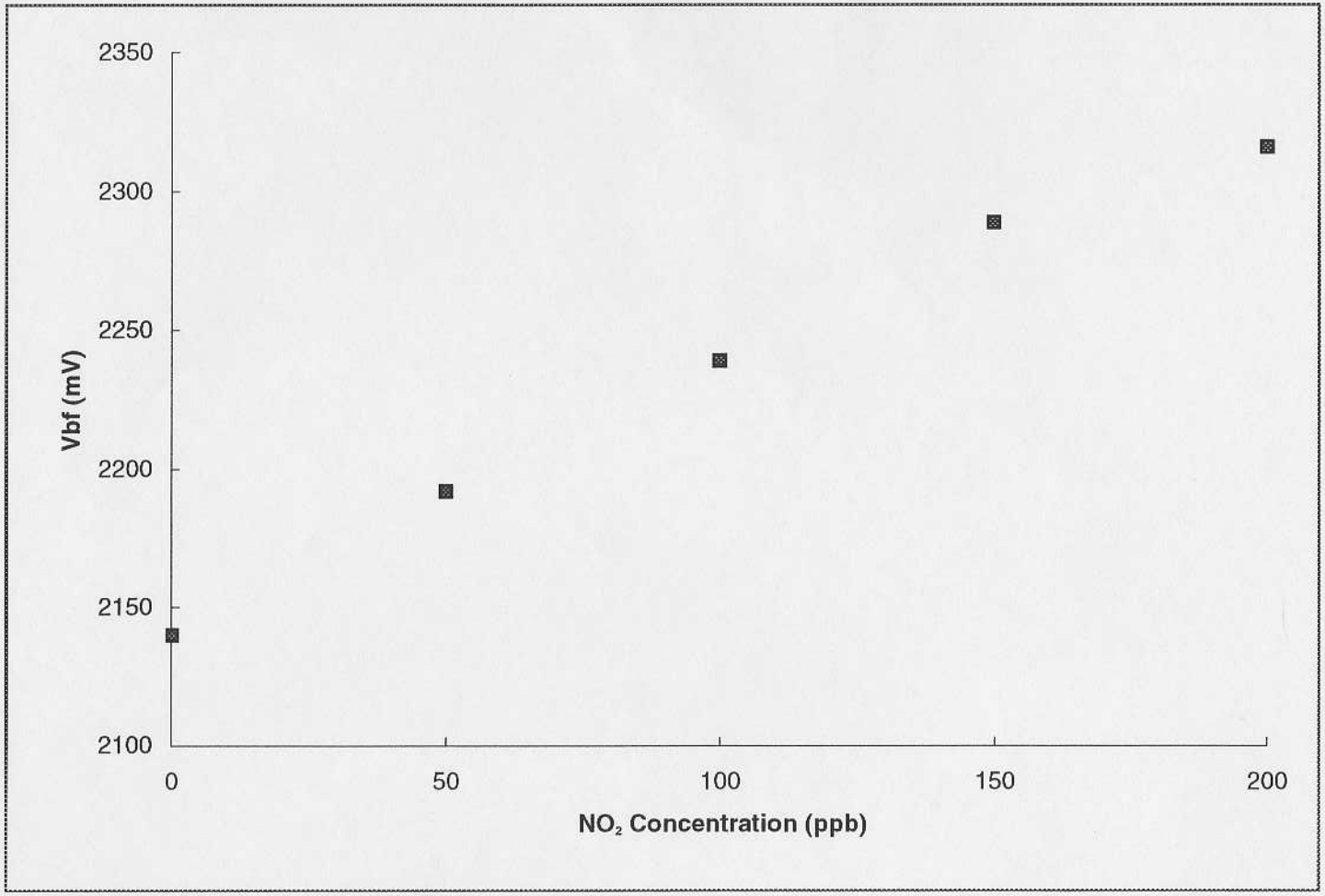
2350
2300
2250
2200
2150
2100
Vbf (mV)
0
50
100
150
200
NO2 Concentration (ppb)

Figure 5